EUROPEAN COOPERATION
IN THE FIELD OF SCIENTIFIC
AND TECHNICAL RESEARCH

EURO-COST

SOURCE: *Graz University of Technology

IC1004 TD(13)07012
Illmenau, Germany
May 28-31, 2013

Performance Bounds for Multipath-assisted Indoor Localization on Backscatter Channels

Erik Leitinger*, Paul Meissner*, Markus Fröhle*, Klaus Witrisal*
Inffeldgasse 16c
A-8010 Graz
Austria
Phone: +43 316 873 4364
Fax: +43 316 873 104364
Email: erik.leitinger@tugraz.at

Performance Bounds for Multipath-assisted Indoor Localization on Backscatter Channels

Erik Leitinger*, Paul Meissner*, Markus Fröhle*, and Klaus Witrisal*
*Graz University of Technology, Inffeldgasse 16c, A-8010 Graz, Austria, email: erik.leitinger@tugraz.at

***Abstract*—In this paper, we derive the Cramer-Rao lower bound (CRLB) on the position error for an RFID tag positioning system exploiting multipath. The channels constituting the backscatter radio system are modeled with a hybrid deterministic/stochastic channel model. In this way, both the geometry of the deterministic multipath components (MPCs) and the diffuse multipath are taken into account properly. Computational results show the influence of the room geometry on the bound and the importance of the diffuse multipath in dense indoor environments. Time reversal (TR) processing using the deterministic MPCs is analyzed as one possibility to overcome the degenerate nature of the backscatter channel. A derivation and evaluation of the corresponding CRLB shows the potential gain of TR processing as well as its strong dependence on the geometry.**

***Index Terms*—Backscatter channel, Cramér-Rao lower bound, Ultra-wideband, multipath-assisted indoor localization**

I. Introduction

Ultra-wideband signals are promising candidates for localization in harsh indoor multipath environments, due to fine time-resolution enabled by large bandwidth. Nevertheless, indoor positioning is still a challenging task, in particular due to errors caused by non-line-of-sight (NLOS) propagation conditions. These problems appear even more stronger in backscatter channels used for localization of RFID tags.

Performance bounds such as the Cramer-Rao lower bound (CRLB) can yield insights on the influence of the channel parameters on the localization accuracy. In references like [1]–[3] the squared position error bound (SPEB) given by the information inequality is derived directly from the entire received signal rather than from specific features extracted from the signal. If floor-plan information is available, multipath components (MPCs) associated to strong reflections, can increase the information for the positioning estimation [4]. These MPCs can be seen as originated from so-called virtual anchors (VAs) as shown in Fig. 1. A key difference in [4] to [1]–[3] is the explicit modeling of the diffuse multipath (DM) using a stochastic process. These theoretical results were verified using data from an extensive indoor measurement campaign [5].

The contribution of this paper is the extension of the theoretical framework in [4] to the analysis of indoor localization of passive targets via backscatter channels. It is well-known that the channel in backscatter radio systems is degenerate pinhole channel [6], formed by the concatenation

This work was partly supported by the Austrian Science Fund (FWF) within the National Research Network SISE project S10610.

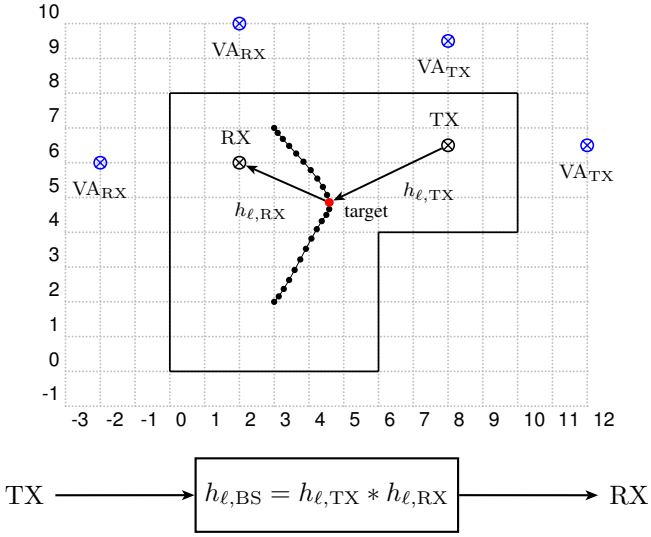

Fig. 1: Top: Floorplan with a transmitter (TX) and receiver (RX) radar node and a subset of corresponding VAs. The up-link is the channel between TX and the target at position ℓ, the down-link is the channel between the target and RX. Bottom: Backscatter model as concatenation of a up- and down-link channels.

of the channel from the transmitter TX to the target and from the target to the receiver RX. A comprehensive theoretical analysis and calculation of PDP and the backscatter channel parameters can be found in [6].

Time-reversal processing (TR) [7], [8] for backscatter channels has been motivated in [9], where it is applied on the channel to focus the energy at RFID tags on a certain position and to separate the up- and down-link channels from one another. Common TR processing uses the entire reversed complex conjugate channel. This is not resilient w.r.t. imperfect channel knowledge, as any errors cause incoherent summation of paths and thereby loss of focusing of the energy. Therefore, we only use a limited set of deterministic MPCs that can be modeled geometrically, as these have been shown to carry a large fraction of the channel energy [10]. Due to this, we analyze in our work the impact of TR processing on the CRLB for multipath-assisted indoor positioning.

This paper is organized as follows: In Section II the backscatter channel model is given and the signaling for TR processing is discussed. The derivation of the CRLB of the position error on the backscatter channel is provided in Section III. Results are given in Section IV. Finally, in Section V a conclusion is given.

II. Signal and Channel Model

A. Hybrid Deterministic-Stochastic Channel

The hybrid deterministic-stochastic complex baseband radio channel $h_{m,\ell}(\tau)$ between a radar node $m \in \{\mathrm{TX}, \mathrm{RX}\}$ located at position $\mathbf{p}_{1,m}$ and a target at position $\mathbf{p}_\ell$ is defined as

$$h_{m,\ell}(\tau) = \sum_{k=1}^{K_{m,\ell}} \alpha_{k,m,\ell}\delta(\tau - \tau_{k,m,\ell}) + \nu_{m,\ell}(\tau) \qquad (1)$$

where the first term consists of $K_{m,\ell}$ deterministic MPCs with complex amplitude $\alpha_{k,m,\ell} \in \mathbb{C}$ and delay $\tau_{k,m,\ell} = \frac{1}{c}||\mathbf{p}_\ell - \mathbf{p}_{k,m}||$, where c is the speed of light. The delays of deterministic MPCs, i.e. strong specular reflections on surfaces can be modeled geometrically, if the floor-plan is known a-priori. Fig. 1 shows the location $\left\{\mathbf{p}_{k,m} = [x_{k,m}, y_{k,m}]^T\right\}_{k=0}^{K_{m,\ell}}$ of a subset of VAs in the considered environment. The second term $\nu_{m,\ell}(\tau)$ denotes the diffuse multipath (DM) and is modeled with a stochastic process. We assume uncorrelated scattering (US), which means that contributions of the DM with different delays are uncorrelated, so that the ACF of the DM is given as

$$\begin{aligned} K_\nu(\tau, u) &= \mathbb{E}\left\{\nu_{m,\ell}(\tau)\nu_{m,\ell}(u)^*\right\} \\ &= S_{\nu,m,\ell}(\tau - \tau_{1,m,\ell})\delta(\tau - u). \end{aligned} \qquad (2)$$

$S_{\nu,m,\ell}(\tau - \tau_{1,m,\ell})$ is the power delay profile (PDP), where $S_{\nu,m,\ell} = 0$ for $\tau < \tau_{1,m,\ell}$, which implies that the DM does not exist until the first deterministic MPC excites the channel. For a specific radar node m and a well defined "local area" around the target position $\mathbf{p}_\ell$ (several wavelengths), DM is assumed to be quasi-stationary, which is given if the channel's first- and second-order statistics do not change noticeably in the spatial domain [11].

B. Backscatter Channel

For brevity, we drop the position index ℓ in further derivations. The backscatter CIR is obtained by the convolution of the up- and down link channels both modeled with (1)

$$\begin{aligned} h_{\mathrm{BS}}(\tau) &= h_{\mathrm{TX}}(\tau) * h_{\mathrm{RX}}(\tau) \\ &= \sum_{k=1}^{K_{\mathrm{TX}}}\sum_{l=1}^{K_{\mathrm{RX}}} \alpha_{k,\mathrm{TX}}\alpha_{l,\mathrm{RX}}\delta(\tau - \tau_{k,\mathrm{TX}} - \tau_{l,\mathrm{RX}}) \\ &+ \sum_{k=1}^{K_{\mathrm{TX}}} \alpha_{k,\mathrm{TX}}\nu_{\mathrm{RX}}(\tau - \tau_{k,\mathrm{TX}}) + \sum_{l=1}^{K_{\mathrm{RX}}} \alpha_{l,\mathrm{RX}}\nu_{\mathrm{TX}}(\tau - \tau_{l,\mathrm{RX}}) \\ &+ \nu_{\mathrm{TX}}(\tau) * \nu_{\mathrm{RX}}(\tau). \end{aligned} \qquad (3)$$

Here, the first term is denoted as $h_{\mathrm{BS,det}}(\tau)$, which represents the deterministic part of the backscatter channel. The second and third term are the convolution of the DM of the up-link channel with the deterministic components of the down-link channel, and vice versa. The last term constitutes the convolution of the DM of the up- and down-link channels. In the following, we denote the sum of the last three terms of (3) that comprise the DM as $\nu_{\mathrm{BS}}(\tau) = \nu_{\mathrm{TX,DM_{RX}}}(\tau) + \nu_{\mathrm{RX,DM_{TX}}}(\tau) + \nu_{\mathrm{DM_{TX},DM_{RX}}}(\tau)$. From (3) it is seen that the backscatter channel can be decomposed into a deterministic and a diffuse part, in the same way as the up- and down-links in (1). With the quasi-stationarity and US assumption, the PDP of the backscatter channel is the second central moment of the DM process

$$\begin{aligned} S_{\nu,\mathrm{BS}}(\tau) &= \mathbb{E}\left\{\nu_{\mathrm{BS}}(\tau)\nu_{\mathrm{BS}}^*(\tau)\right\} \\ &= \mathbb{E}\left\{\sum_{k=1}^{K_{\mathrm{TX}}}\sum_{k'=1}^{K_{\mathrm{TX}}} \alpha_{k,\mathrm{TX}}\alpha_{k',\mathrm{TX}}^*\nu_{\mathrm{RX}}(\tau - \tau_{k,\mathrm{TX}})\nu_{\mathrm{RX}}^*(\tau - \tau_{k',\mathrm{TX}})\right\} \\ &+ \mathbb{E}\left\{\sum_{l=1}^{K_{\mathrm{RX}}}\sum_{l'=1}^{K_{\mathrm{RX}}} \alpha_{l,\mathrm{RX}}\alpha_{l',\mathrm{RX}}^*\nu_{\mathrm{TX}}(\tau - \tau_{l,\mathrm{RX}})\nu_{\mathrm{TX}}^*(\tau - \tau_{l',\mathrm{RX}})\right\} \\ &+ \mathbb{E}\left\{\nu_{\mathrm{TX}}(\tau) * \nu_{\mathrm{RX}}(\tau)(\nu_{\mathrm{TX}}(\tau) * \nu_{\mathrm{RX}}(\tau))^*\right\}. \end{aligned} \qquad (4)$$

We assume a zero-mean Gaussian model for the DM, thus first and second moments give a complete description of the random process. The validity of the US assumption for a backscatter channel constituted by two US-channels has been proven in the appendix of [6], which leads to

$$\begin{aligned} S_{\nu,\mathrm{BS}}(\tau) &= \sum_{k=1}^{K_{\mathrm{TX}}} |\alpha_{k,\mathrm{TX}}|^2 S_{\nu,\mathrm{RX}}(\tau - \tau_{k,\mathrm{TX}}) \\ &+ \sum_{l=1}^{K_{\mathrm{RX}}} |\alpha_{l,\mathrm{RX}}|^2 S_{\nu,\mathrm{TX}}(\tau - \tau_{l,\mathrm{RX}}) + S_{\nu,\mathrm{TX}}(\tau) * S_{\nu,\mathrm{RX}}(\tau). \end{aligned} \qquad (5)$$

In Fig. 2(a) the deterministic MPCs and the PDPs of the DM of some exemplary up- and down-link channels are shown. Fig. 2(b) shows the deterministic components $h_{\mathrm{BS,det}}(\tau)$ and the individual terms of the PDP $S_{\nu,\mathrm{BS}}(\tau)$ of the backscatter channel as described by (5). The solid gray lines denote the PDPs of the DM of the down-link channel $\nu_{\mathrm{RX}}(\tau)$ shifted and scaled by the deterministic components of the up-link channel, the dashed gray lines denote the PDPs of the DM of the up-link channel $\nu_{\mathrm{TX}}(\tau)$ shifted and scaled by the deterministic components of the down-link channel and the dotted gray lines indicates the convolution of the PDPs of the up- and down-link channel. It is seen that the convolution results in higher DM contribution in the BS channel.

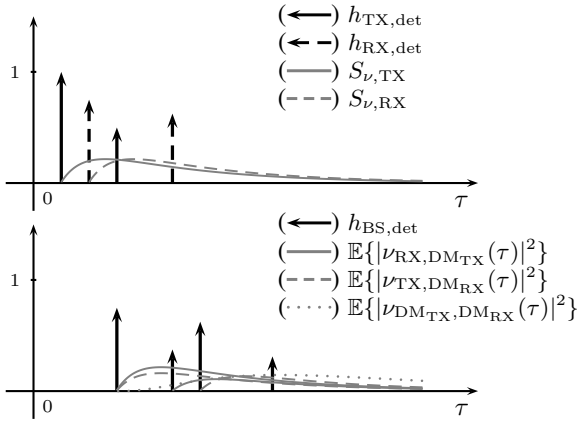

Fig. 2: (a) Up- and down-link channel. Solid lines denote the up-link channel, with deterministic components in black and the PDPs of the DM in gray. Dashed lines indicate the down-link channel. (b) Backscatter channel. Solid black lines denote the deterministic components. The gray lines indicate the different summands of the PDP as described in (5).

C. Transmitted Signal – Time-Reversal Processing

We assume that the TX transmits a signal $s(t) \in \mathbb{C}$. On the one hand, this can be a commonly used raised cosine pulse $p(t)$ with pulse duration T_p. Hence, the received signal represents the backscatter channel convolved with this pulse $p(t)$. On the other hand, the transmitted signal $s(t)$ can be a complex weighted sum of time-shifted copies of this pulse $p(t)$ in order to obtain a TR signal.

TR processing is one promising candidate to overcome the degenerate pinhole nature of the backscatter channel, because it optimizes the link-budget between the TX and RX by focusing the energy onto the target. This is done by using the deterministic MPCs of $h_{\mathrm{TX}}(\tau)$ in (1), which are geometrically modeled by the VAs, as a virtual antenna array for spatial focusing. Combining the estimated parameters of these MPCs in a hypothetical TR-channel, the TX signal becomes

$$\begin{aligned} s(t) = h_{\mathrm{TR}}(t) * p(t) &= \sum_{k=1}^{\hat{K}_{\mathrm{TX}}} \hat{\alpha}_{k,\mathrm{TX}}^{*} \delta\big(t + \hat{\tau}_{k,\mathrm{TX}}\big) * p(t) \\ &= \sum_{k=1}^{\hat{K}_{\mathrm{TX}}} \hat{\alpha}_{k,\mathrm{TX}}^{*} p\big(t + \hat{\tau}_{k,\mathrm{TX}}\big) \end{aligned} \tag{6}$$

where $\{\hat{\alpha}_{k,\mathrm{TX}},\ \hat{\tau}_{k,\mathrm{TX}}\}$ is the set of $\hat{K}_{\mathrm{TX}}$ estimated MPCs of the up-link channel h_{TX} for a position $\hat{\mathbf{p}}$. The normalized complex amplitudes are then given by $\hat{\alpha}_{k,\mathrm{TX}} = \alpha_{k,\mathrm{TX}}/\sqrt{E_{\mathrm{TR}}}$, where $E_{\mathrm{TR}} = \int_{-\infty}^{\infty} |s(t)|^2 \mathrm{d}t$.

The received signal at radar node RX can be obtained by the convolution of (3) with the transmit waveform (6) and AWGN $n(t)$ with a two-sided power spectral density of $N_0/2$

$$\begin{aligned} r(t) &= s(t) * h_{\mathrm{BS}}(t) + n(t) \\ &= \big[h_{\mathrm{TR}}(t) * h_{\mathrm{BS,det}}(t) + h_{\mathrm{TR}}(t) * \nu_{\mathrm{BS}}(t)\big] * p(t) + n(t) \\ &= \Big[\sum_{k=1}^{K_{\mathrm{TX}}} \sum_{l=1}^{K_{\mathrm{RX}}} \sum_{k'=1}^{\hat{K}_{\mathrm{TX}}} \alpha_{k,\mathrm{TX}} \alpha_{l,\mathrm{RX}} \hat{\alpha}_{k',\mathrm{TX}}^{*} \\ &\qquad \times \delta(t - \tau_{k,\mathrm{TX}} - \tau_{l,\mathrm{RX}} + \hat{\tau}_{k',\mathrm{TX}}) \\ &\quad + \sum_{k=1}^{K_{\mathrm{TX}}} \sum_{k'=1}^{\hat{K}_{\mathrm{TX}}} \alpha_{k,\mathrm{TX}} \hat{\alpha}_{k',\mathrm{TX}}^{*} \nu_{\mathrm{RX}}(t - \tau_{k,\mathrm{TX}} + \hat{\tau}_{k',\mathrm{TX}}) \\ &\quad + \sum_{l=1}^{K_{\mathrm{RX}}} \sum_{k'=1}^{\hat{K}_{\mathrm{TX}}} \alpha_{l,\mathrm{RX}} \hat{\alpha}_{k',\mathrm{TX}}^{*} \nu_{\mathrm{TX}}(t - \tau_{l,\mathrm{RX}} + \hat{\tau}_{k',\mathrm{TX}}) \\ &\quad + \int \sum_{k'=1}^{\hat{K}_{\mathrm{TX}}} \hat{\alpha}_{k',\mathrm{TX}}^{*} \nu_{\mathrm{TX}}(\lambda) \nu_{\mathrm{RX}}(t + \hat{\tau}_{k',\mathrm{TX}} - \lambda) \mathrm{d}\lambda \Big] * p(t) + n(t). \end{aligned} \tag{7}$$

The first term comprises deterministic components of the received signal $r(t)$, and the remaining terms constitute the DM arriving at the RX. Eq. (7) again shows that the channel described by the convolution of $h_{\mathrm{BS}}(\tau)$ and $h_{\mathrm{TR}}(\tau)$ can be decomposed into deterministic and diffuse parts. Assuming perfect TR parameters are available, (7) gives additional insights in the TR processing: First, the energy is concentrated on the deterministic MPCs of the down-link channel $h_{\ell,\mathrm{RX}}(\tau)$. Second, again the structure of an equivalent deterministic channel and DM can be observed. The PDP of the received DM can be obtained as

$$\begin{aligned} &S_{\nu,\mathrm{TR}}(\tau) = \\ &= \sum_{k=1}^{K_{\mathrm{TX}}} \sum_{k'=1}^{\hat{K}_{\mathrm{TX}}} |\alpha_{k,\mathrm{TX}}|^2 |\hat{\alpha}_{k',\mathrm{TX}}|^2 S_{\nu,\mathrm{RX}}(\tau - \tau_{k,\mathrm{TX}} + \hat{\tau}_{k',\mathrm{TX}}) \\ &+ \sum_{l=1}^{K_{\mathrm{RX}}} \sum_{k'=1}^{\hat{K}_{\mathrm{TX}}} |\alpha_{l,\mathrm{RX}}|^2 |\hat{\alpha}_{k',\mathrm{TX}}|^2 S_{\nu,\mathrm{TX}}(\tau - \tau_{l,\mathrm{RX}} + \hat{\tau}_{k',\mathrm{TX}}) \\ &+ \sum_{k'=1}^{\hat{K}_{\mathrm{TX}}} |\hat{\alpha}_{k',\mathrm{TX}}|^2 \int_{-\infty}^{\infty} S_{\nu,\mathrm{TX}}(\lambda) S_{\nu,\mathrm{RX}}(\tau + \hat{\tau}_{k',\mathrm{TX}} - \lambda) \mathrm{d}\lambda. \end{aligned} \tag{8}$$

III. Error Bound on the Position Estimation

In this section, we derive the Equivalent Fisher Information Matrix (EFIM) [2] of the target via the backscatter channel. The derivation and the notation follow closely [3] and [4]. Additionally, the influence of TR processing on the bound is analyzed.

A. Problem Formulation

Our goal is to estimate the position $\mathbf{p}$ of the target, using the knowledge of the position of the TX- and RX-base station at positions $\mathbf{p}_{1,\mathrm{TX}}$ and $\mathbf{p}_{1,\mathrm{RX}}$, in the presence of DM and AWGN. With a-priori known floor-plan information, they span two corresponding sets of VAs at positions $\{\mathbf{p}_{k,\mathrm{TX}}\}$ and $\{\mathbf{p}_{k,\mathrm{RX}}\}$. For the sake of simplicity, we introduce for the backscatter channel the equivalent propagation delays $\tau_{k,l} = \tau_{k,\mathrm{TX}} + \tau_{l,\mathrm{RX}} = \frac{1}{c}||\mathbf{p} - \mathbf{p}_{k,\mathrm{TX}}|| + \frac{1}{c}||\mathbf{p} - \mathbf{p}_{l,\mathrm{RX}}||$, which are related to the geometry. Their corresponding complex amplitudes $\alpha_{k,l} = \alpha_{k,\mathrm{TX}} \alpha_{l,\mathrm{RX}}$ are nuisance parameters for the position estimation.

The CRLB on the position error provides a lower bound for the MSE on an unbiased estimator and is computed as the inverse of the Fisher Information Matrix (FIM) $\mathbf{J}(\boldsymbol{\theta})$ [12]. The vector of unknown parameters for position estimation is defined as $\boldsymbol{\theta} = \big[\mathbf{p}^{\mathrm{T}}\ (\boldsymbol{\alpha}^{\mathrm{R}})^{\mathrm{T}}\ (\boldsymbol{\alpha}^{\mathrm{I}})^{\mathrm{T}}\big]^{\mathrm{T}}$ and the transformed parameter vector, related to the received signal $r(t)$, is $\boldsymbol{\psi} = \big[\boldsymbol{\tau}^{\mathrm{T}}\ (\boldsymbol{\alpha}^{\mathrm{R}})^{\mathrm{T}}\ (\boldsymbol{\alpha}^{\mathrm{I}})^{\mathrm{T}}\big]^{\mathrm{T}}$. The FIM for position estimation is computed by applying the chain rule

$$\mathbf{J}(\boldsymbol{\theta}) = \mathbf{P} \mathbf{J}(\boldsymbol{\psi}) \mathbf{P}^{\mathrm{T}} \tag{9}$$

where $\mathbf{P} = \partial\boldsymbol{\psi}/\partial\boldsymbol{\theta}$ is the the Jacobian Matrix of the transformation. The FIM of the transformed parameter vector $\boldsymbol{\psi}$ is defined as

$$\mathbf{J}(\boldsymbol{\psi}) = \mathbb{E}_{\mathbf{r}|\boldsymbol{\psi}} \left\{ -\frac{\partial^2}{\partial\boldsymbol{\psi}\partial\boldsymbol{\psi}} \ln \mathrm{p}(\mathbf{r}|\boldsymbol{\psi}) \right\} \tag{10}$$

where the observation vector $\mathbf{r}$ is obtained from the Karhunen-Loéve expansion of the received signal $r(t)$ [12].

B. Likelihood Function of the Received Signal

The likelihood function we use is adopted from [4]. Due to the fact that the DM $\nu_{\ell,\mathrm{BS}}(\tau)$ in (7), convolved with the transmitted signal $s(t)$, is described as a colored Gaussian noise process, a whitening operation has to be applied to the received signal $r(t)$ to obtain a tractable likelihood function.

Given that the backscatter channel and the TR processed backscatter channel are both composed the same way as the channel used in [4], the framework to derive the likelihood function can be extended to the backscatter channel, so that we can write

$$\ln \mathrm{p}(\mathbf{r}|\boldsymbol{\psi}) \propto \frac{2}{N_0}\int_0^{T_{\mathrm{ob}}} \Re\Big\{ r(t) \sum_{k=1}^{K_{\mathrm{TX}}}\sum_{l=1}^{K_{\mathrm{RX}}} w_{k,l}^2 \alpha_{k,l}^* s^*(t-\tau_{k,l})\Big\}\mathrm{d}t - \frac{1}{N_0}\int_0^{T_{\mathrm{ob}}} \Big| \sum_{k=1}^{K_{\mathrm{TX}}}\sum_{l=1}^{K_{\mathrm{RX}}} w_{k,l}\alpha_{k,l} s(t-\tau_{k,l})\Big|^2 \mathrm{d}t \quad (11)$$

where T_{ob} is the observation time and $w_{k,l} = \sqrt{N_0/(N_0 + T_p S_\nu(\tau_{k,l}))}$ are the weighting factors accounting for DM. $S_\nu(\tau_{k,l})$, denotes the PDP of the backscatter channel alone or with TR-processing. The term $T_p S_\nu(\tau_{k,l})$ constitutes the power of the DM c.f. (5) and (8). The signal $s(t) \in \mathbb{C}$ either represents the TR waveform or the baseband signal $p(t)$.

C. EFIM and SPEB

The MSE of the position and the FIM are related to the information inequality [12]

$$\mathbb{E}_{\mathbf{r}|\boldsymbol{\theta}}\{||\hat{\mathbf{p}} - \mathbf{p}||^2\} \geq \mathrm{tr}\{[\mathbf{J}(\boldsymbol{\theta})_{2\times 2}]^{-1}\} \quad (12)$$

where $\mathrm{tr}\{\cdot\}$ is the trace of a square matrix. $\mathbf{J}(\boldsymbol{\theta})_{2\times 2}$ is the upper left submatrix, which comprises the information on the position estimation and is called EFIM [2]. It leads to a reduction of the dimensionality of the FIM. $\hat{\mathbf{p}}$ is the position estimate based on the observation vector $\mathbf{r}$. The SPEB at position $\mathbf{p}$ is defined as

$$\mathcal{P}(\mathbf{p}) \equiv \mathrm{tr}\{[\mathbf{J}(\boldsymbol{\theta})_{2\times 2}]^{-1}\} \quad (13)$$

and represents the CRLB on the position error. The matrix $\mathbf{P}$ for the parameter transformation in (9) is

$$\mathbf{P} = \begin{bmatrix} \mathbf{H}_{2\times K_{\mathrm{TX}}K_{\mathrm{RX}}} & \mathbf{0}_{2\times 2K_{\mathrm{TX}}K_{\mathrm{RX}}} \\ \mathbf{0}_{K_{\mathrm{TX}}K_{\mathrm{RX}}2\times 2} & \mathbf{I}_{2K_{\mathrm{TX}}K_{\mathrm{RX}}\times 2K_{\mathrm{TX}}K_{\mathrm{RX}}} \end{bmatrix} \quad (14)$$

where $\mathbf{0}$ is the zero matrix, $\mathbf{I}$ is the identity matrix and $\mathbf{H}$ incorporates the geometry. The columns of $\mathbf{H}$ are of the form $-\frac{1}{c}[\cos\phi_{k,\mathrm{TX}} + \cos\phi_{l,\mathrm{RX}},\ \sin\phi_{k,\mathrm{TX}} + \sin\phi_{l,\mathrm{RX}}]^{\mathrm{T}}$, where $\phi_{k,\mathrm{TX}}$ and $\phi_{l,\mathrm{RX}}$ are the angles between VAs of the TX- and RX-radar node and the target. For example on the TX side, this angle is defined as $\phi_{k,\mathrm{TX}} = \tan^{-1}((y - y_{k,\mathrm{TX}})/(x - x_{k,\mathrm{TX}}))$. The EFIM on the position error can be written as [4]

$$\mathrm{EFIM} \equiv \mathbf{J}(\boldsymbol{\theta})_{2\times 2} = \mathbf{H}\boldsymbol{\Lambda}_{\mathrm{A}}\mathbf{H}^{\mathrm{T}} - \mathbf{H}\boldsymbol{\Lambda}_{\mathrm{B}}\boldsymbol{\Lambda}_{\mathrm{C}}^{-1}\boldsymbol{\Lambda}_{\mathrm{B}}^{\mathrm{T}}\mathbf{H}^{\mathrm{T}} \quad (15)$$

where the block matrices $\boldsymbol{\Lambda}_{\mathrm{A}}$, $\boldsymbol{\Lambda}_{\mathrm{B}}$ and $\boldsymbol{\Lambda}_{\mathrm{C}}$ are defined in the appendix. If there is no path overlap, $\boldsymbol{\Lambda}_{\mathrm{A}}$ is a diagonal matrix and $\boldsymbol{\Lambda}_{\mathrm{B}}$ is zero. According to [4], the EFIM can then be written in a canonical form as

$$\mathbf{J}(\boldsymbol{\theta})_{2\times 2} = \frac{8\pi^2\beta^2}{c^2}\sum_{k=1}^{K_{\mathrm{TX}}}\sum_{l=1}^{K_{\mathrm{RX}}} \mathrm{SINR}_{k,l}\mathbf{J}_{\mathrm{r}}(\phi_k,\phi_l) \quad (16)$$

where β^2 is the mean squared bandwidth of the pulse $p(t)$,

$$\mathrm{SINR}_{k,l} = w_{k,l}^2\frac{|\alpha_{k,l}|^2}{N_0} = \frac{|\alpha_{k,l}|^2}{N_0 + T_p S_\nu(\tau_{k,l})} \quad (17)$$

is the signal-to-interference-plus-noise ratio of the k,l-th backscatter MPC and

$$\mathbf{J}_{\mathrm{r}}(\phi_k,\phi_l) = \begin{bmatrix} \mathrm{A}^2 & \mathrm{AB} \\ \mathrm{AB} & \mathrm{B}^2 \end{bmatrix} \quad (18)$$

is the 2×2 ranging direction matrix accounting for the geometry, where $\mathrm{A} = \cos\phi_{k,\mathrm{TX}} + \cos\phi_{l,\mathrm{RX}}$ and $\mathrm{B} = \sin\phi_{k,\mathrm{TX}} + \sin\phi_{l,\mathrm{RX}}$. Note that (16) in general does not hold for backscatter channels with TR processing, due to additional generated overlap of signal paths.

This analytical result was comprehensively analyzed for the single-channel MINT scenario in [4]. There, the main findings which also are evident in (16) are the following. First, any increase of the effective bandwidth decreases the SPEB. Second, each additional VA increases the EFIM and consequently decreases the SPEB, and third, the gain of each VA is determined by the corresponding SINR.

D. Influence of TR Processing on the Position Error Bound

One impact of TR processing on the CRLB is that the weights $w_{k,l}$ accounting for the DM change according to the PDP $S_{\nu,\mathrm{TR}}$. Furthermore, TR processing influences the signal correlation function, which appears in the block matrices of the EFIM (c.f. appendix), the following way

$$\begin{aligned} \mathrm{R}_s(\tau_{k,l} - \tau_{k',l'}) &= \int_{-\infty}^{\infty} s(t-\tau_{k,l})s(t-\tau_{k',l'})\mathrm{d}t \\ &= \int_{-\infty}^{\infty}\sum_{m=1}^{\hat{K}_{\mathrm{TX}}}\sum_{m'=1}^{\hat{K}_{\mathrm{TX}}} \big|\hat{\alpha}_{m,\mathrm{TX}}\big|^2|\hat{\alpha}_{m',\mathrm{TX}}|^2 \\ &\qquad p(t-\tau_{k,l}+\hat{\tau}_{m,\mathrm{TX}})p(t-\tau_{k',l'}+\hat{\tau}_{m',\mathrm{TX}})\mathrm{d}t \\ &= \sum_{m=1}^{\hat{K}_{\mathrm{TX}}}\sum_{m'=1}^{\hat{K}_{\mathrm{TX}}} \big|\hat{\alpha}_{m,\mathrm{TX}}\big|^2|\hat{\alpha}_{m',\mathrm{TX}}|^2 \\ &\qquad \mathrm{R}_p((\tau_{k,l}-\hat{\tau}_{m,\mathrm{TX}}) - (\tau_{k',l'}-\hat{\tau}_{m',\mathrm{TX}})). \end{aligned} \quad (19)$$

where $\mathrm{R}_p(\tau_{k,l} - \tau_{k',l'}) = \int_{-\infty}^{\infty} p(t-\tau_{k,l})p(t-\tau_{k',l'})\mathrm{d}t$ is the ACF of the transmitted pulse $p(t)$. Eq. (19) illustrates the additional generated path overlap by TR processing.

IV. Results

1) Simulation Setup: A computational analysis has been performed for the scenario illustrated in Fig. 3 for a target that move along a trajectory consisting of 24 target positions. The TX radar node is located at position $\mathrm{p}_{1,\mathrm{TX}} = [8,\ 7.5]^{\mathrm{T}}$ and the RX radar node at position $\mathrm{p}_{1,\mathrm{RX}} = [2,\ 6]^{\mathrm{T}}$. Deterministic MCPs of the up- and down-link channels $h_{\mathrm{TX}}(\tau)$ and $h_{\mathrm{RX}}(\tau)$ have been generated using corresponding first- and second-order VAs together with the LOS components. A similar path-loss model for carrier frequency of 7 GHz as in [4] has been used for the MPC gains, adding 3 dB of attenuation for each reflection order. The ACF $R_p(\tau)$ of the transmitted signal $p(t)$ is modeled as raised cosine pulse, with a roll-off factor $\beta_{\mathrm{roll}} = 0.6$ and pulse duration of $T_p = 0.5$ ns corresponding

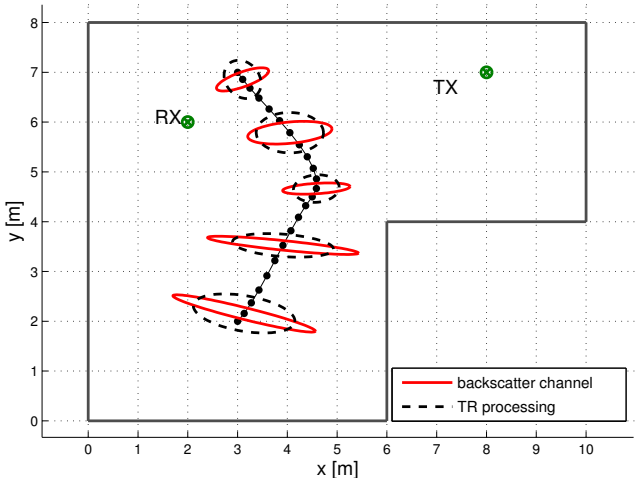

Fig. 3: Simulation scenario. Position error ellipses of the forty-fold standard deviation.

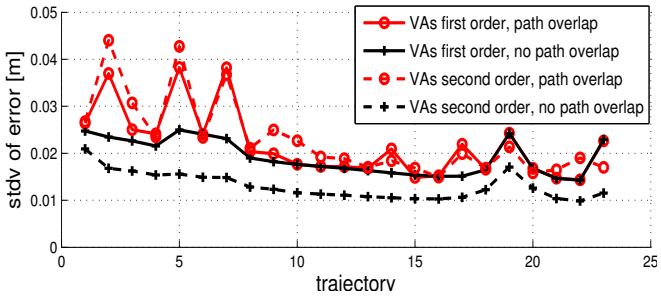

Fig. 4: Position error bound along a trajectory for backscatter channel for VA order 1 and 2, with and without path overlap.

to a bandwidth of 2 GHz. The PDP of the diffuse part of both channels are modeled as double-exponential function cf. [13, (9)]. Its parameters are the total power of the diffuse multipath $\Omega_1 = 1.16 \times 10^{-6}$, $\gamma_1 = 20$ ns, $\gamma_{\text{rise}} = 5$ ns and $\chi = 0.98$, which were kept fixed over the entire floorplan. However, due to the concatenation of the up- and down-link channels, the resulting backscatter channel PDP of the DM depends on both channel's deterministic parts, i.e. on the target position. The SNR of DM varies along the trajectory between 25 dB and 31 dB. The SINR of the LOS at first the trajectory position $\mathbf{p} = [3, 2]$ is 21 dB for the backscatter channel and 15 dB for the backscatter channel with TR processing.

2) CRLB for Backscatter channel and Influence of TR processing: Due to the fact that in backscatter channel more MPCs appear than in one single channel, path-overlap is more probable, which causes stronger degeneration of the PEB. This is illustrated in Fig. 4, where the PEB is computed from the complete EFIM (15) and the canonical form (16) for first-order reflections (red lines) and for second-order reflections (black lines). We can see that on the one hand, the PEB neglecting path overlap is decreasing with increasing number of MPCs, but on the other hand, the PEB considering path overlap is partly increasing.

Fig. 3 shows the position error ellipses for the forty-fold

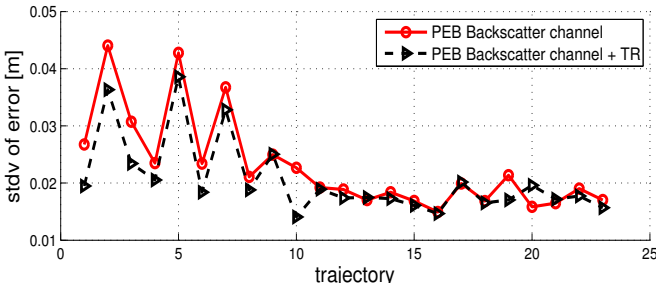

(a) LOS, VA order 1 for TR processing

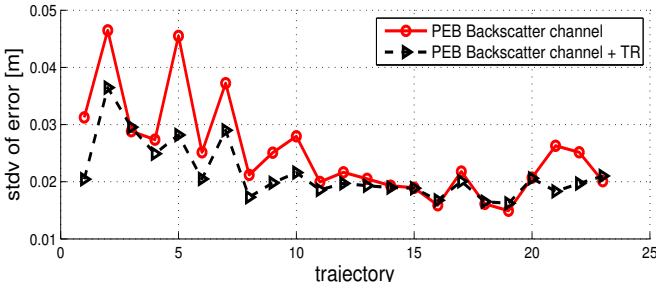

(b) NLOS, VA order 1 for TR processing

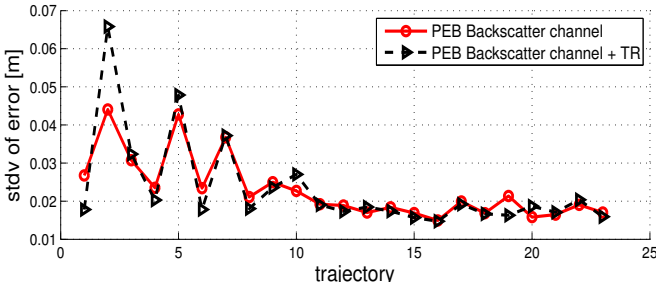

(c) LOS, VA order 2 for TR processing

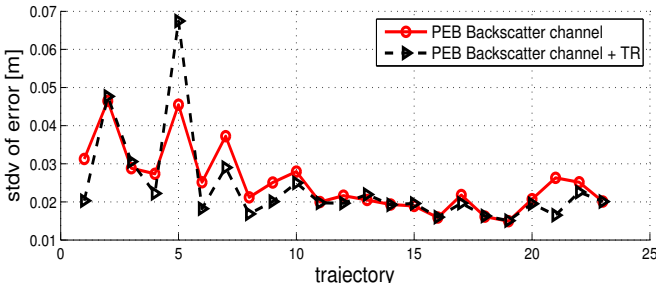

(d) NLOS, VA order 2 for TR processing

Fig. 5: Position error bound along a trajectory for LOS and NLOS scenarios with VA order of 1 and 2 for TR processing (path overlap considered).

standard deviation for several trajectory positions, in red for the backscatter channel alone and in black (dashed) with TR processing. Here, one can see that the error depends on the geometry and it is lower in the direction of the TX and RX radar nodes, because MPCs from other directions are strongly impaired by DM. Another interesting fact is that TR processing partly levels this imbalance. It improves the information from reflected MPCs, while loosing information from the LOS component, which gets also affected by DM due to TR processing. However, the overall PEB is decreasing

for TR processing for most positions, but the gain depends strongly on the geometry and can also get negative.

Figs. 5(a)-(d) show the PEB of the backscatter channel with TR processing along the trajectory for the LOS and NLOS cases (path overlap considered), where the latter means that the first component of the TX channel has been set to zero. Figs. 5(a) and (b) illustrate TR processing with MPCs coming from VAs of first-order. One can see that TR processing results in a performance gain, especially for NLOS scenarios. As Figs. 5(c) and (d) show, the inclusion of second-order reflections in TR parameter set does not automatically yields in a performance gain. This can be explained by the fact that the impairment of additional DM is higher than the gain caused by energy focusing. The results illustrate again that the performance gain through TR processing is strongly dependent on the geometry of the room.

V. Conclusions

Using a channel model that explicitly models the diffuse multipath, a unified likelihood model for the localization can be used independently of whether TR processing is used or not. Results show the detrimental effect of path overlap in backscatter channels on the PEB. Using geometrically modeled deterministic MPCs for TR processing does not automatically imply large performance gains. The special structure of DM in the backscatter channel suggest a careful usage of a subset of these paths for TR, which is supported by our derivations and results. Ongoing work includes the further analysis on the influence of the selected subsets of MPCs for TR processing and the effect of path overlap on the likelihood function.

Appendix

A. Derivation of the Subblocks of the FIM

The FIM $\mathbf{J}(\boldsymbol{\psi})$ of the transformed parameter vector $\boldsymbol{\psi} = \left[\tau^{\mathrm{T}}\ (\boldsymbol{\alpha}^{\mathrm{R}})^{\mathrm{T}}\ (\boldsymbol{\alpha}^{\mathrm{I}})^{\mathrm{T}}\right]^{\mathrm{T}}$ can be calculated from (10) the following way

$$\mathbf{J}(\boldsymbol{\psi}) = \begin{bmatrix} \boldsymbol{\Lambda}_{\mathrm{A}} & \boldsymbol{\Lambda}_{\mathrm{B}}^{\mathrm{R}} & \boldsymbol{\Lambda}_{\mathrm{B}}^{\mathrm{I}} \\ (\boldsymbol{\Lambda}_{\mathrm{B}}^{\mathrm{R}})^{\mathrm{T}} & \boldsymbol{\Lambda}_{\mathrm{C}}' & \boldsymbol{\Lambda}_{\mathrm{C}}'' \\ (\boldsymbol{\Lambda}_{\mathrm{B}}^{\mathrm{I}})^{\mathrm{T}} & \boldsymbol{\Lambda}_{\mathrm{C}}'' & \boldsymbol{\Lambda}_{\mathrm{C}}' \end{bmatrix}_{3K_{\mathrm{TX}}K_{\mathrm{RX}} \times 3K_{\mathrm{TX}}K_{\mathrm{RX}}} \tag{20}$$

where $\boldsymbol{\Lambda}_{\mathrm{B}} = [\boldsymbol{\Lambda}_{\mathrm{B}}^{\mathrm{R}}\ \boldsymbol{\Lambda}_{\mathrm{B}}^{\mathrm{I}}]$ and $\boldsymbol{\Lambda}_{\mathrm{C}} = [\boldsymbol{\Lambda}_{\mathrm{C}}'\ \boldsymbol{\Lambda}_{\mathrm{C}}''; \boldsymbol{\Lambda}_{\mathrm{C}}''\ \boldsymbol{\Lambda}_{\mathrm{C}}']$. The sub-blocks are derived as

$$\begin{aligned}
[\boldsymbol{\Lambda}_{\mathrm{A}}]_{kl,k'l'} &= \mathbb{E}_{\mathbf{r}|\boldsymbol{\psi}}\left\{\frac{\partial^2 \ln \mathrm{p}(\mathbf{r}|\boldsymbol{\psi})}{\partial\tau_{k,l}\partial\tau_{k',l'}}\right\} \\
&= \frac{2}{N_0} w_{k,l} w_{k',l'} \Re\left\{\alpha_{k,l}\alpha_{k',l'}^{*} \frac{\partial^2 \mathrm{R}_s(\tau_{k,l}-\tau_{k',l'})}{\partial\tau_{k,l}\partial\tau_{k',l'}}\right\} \\
[\boldsymbol{\Lambda}_{\mathrm{B}}^{\mathrm{R}}]_{kl,k'l'} &= \mathbb{E}_{\mathbf{r}|\boldsymbol{\psi}}\left\{\frac{\partial^2 \ln \mathrm{p}(\mathbf{r}|\boldsymbol{\psi})}{\partial\tau_{k,l}\partial\alpha_{k',l'}^{\mathrm{R}}}\right\} \\
&= \frac{2}{N_0} w_{k,l} w_{k',l'} \Re\left\{\alpha_{k,l} \frac{\partial \mathrm{R}_s(\tau_{k,l}-\tau_{k',l'})}{\partial\tau_{k,l}}\right\} \\
[\boldsymbol{\Lambda}_{\mathrm{B}}^{\mathrm{I}}]_{kl,k'l'} &= \mathbb{E}_{\mathbf{r}|\boldsymbol{\psi}}\left\{\frac{\partial^2 \ln \mathrm{p}(\mathbf{r}|\boldsymbol{\psi})}{\partial\tau_{k,l}\partial\alpha_{k',l'}^{\mathrm{I}}}\right\} \\
&= \frac{2}{N_0} w_{k,l} w_{k',l'} \Im\left\{\alpha_{k,l} \frac{\partial \mathrm{R}_s(\tau_{k,l}-\tau_{k',l'})}{\partial\tau_{k,l}}\right\} \\
[\boldsymbol{\Lambda}_{\mathrm{C}}']_{kl,k'l'} &= \mathbb{E}_{\mathbf{r}|\boldsymbol{\psi}}\left\{\frac{\partial^2 \ln \mathrm{p}(\mathbf{r}|\boldsymbol{\psi})}{\partial\alpha_{k,l}^{\mathrm{R}}\partial\alpha_{k',l'}^{\mathrm{R}}}\right\} = \mathbb{E}_{\mathbf{r}|\boldsymbol{\psi}}\left\{\frac{\partial^2 \ln \mathrm{p}(\mathbf{r}|\boldsymbol{\psi})}{\partial\alpha_{k,l}^{\mathrm{I}}\partial\alpha_{k',l'}^{\mathrm{I}}}\right\} \\
&= \frac{2}{N_0} w_{k,l} w_{k',l'} \Re\left\{\mathrm{R}_s(\tau_{k,l}-\tau_{k',l'})\right\} \\
[\boldsymbol{\Lambda}_{\mathrm{C}}'']_{kl,k'l'} &= \mathbb{E}_{\mathbf{r}|\boldsymbol{\psi}}\left\{\frac{\partial^2 \ln \mathrm{p}(\mathbf{r}|\boldsymbol{\psi})}{\partial\alpha_{k,l}^{\mathrm{R}}\partial\alpha_{k',l'}^{\mathrm{I}}}\right\} \\
&= \frac{2}{N_0} w_{k,l} w_{k',l'} \Im\left\{\mathrm{R}_s(\tau_{k,l}-\tau_{k',l'})\right\}
\end{aligned}$$

where $\mathrm{R}_s(\tau_{k,l}-\tau_{k',l'}) = \int_{-\infty}^{\infty} s(t-\tau_{k,l})s(t-\tau_{k',l'})\mathrm{d}t$ is the signal correlation function.

References

[1] Y. Shen and M. Win, "On the use of multipath geometry for wideband cooperative localization," in *Global Telecommunications Conference, 2009. GLOBECOM 2009. IEEE*, Dec. 2009, pp. 1 –6.

[2] ——, "Fundamental limits of wideband localization; part I: A general framework," *Information Theory, IEEE Transactions on*, vol. 56, no. 10, pp. 4956 –4980, Oct. 2010.

[3] H. Godrich, A. Haimovich, and R. Blum, "Target localization accuracy gain in mimo radar-based systems," *Information Theory, IEEE Transactions on*, vol. 56, no. 6, pp. 2783 –2803, June 2010.

[4] K. Witrisal and P. Meissner, "Performance bounds for multipath-assisted indoor navigation and tracking (MINT)," in *Communications (ICC), 2012 IEEE International Conference on*, June 2012, pp. 4321 –4325.

[5] P. Meissner and K. Witrisal, "Analysis of position-related information in measured UWB indoor channels," in *Antennas and Propagation (EUCAP), 2012 6th European Conference on*, March 2012, pp. 6 –10.

[6] D. Arnitz, U. Muehlmann, and K. Witrisal, "Wideband characterization of backscatter channels: Derivations and theoretical background," *Antennas and Propagation, IEEE Transactions on*, vol. 60, no. 1, pp. 257 –266, Jan. 2012.

[7] T. Strohmer, M. Emami, J. Hansen, G. Papanicolaou, and A. Paulraj, "Application of time-reversal with mmse equalizer to UWB communications," in *Global Telecommunications Conference, 2004. GLOBECOM '04. IEEE*, vol. 5, Nov. 2004, pp. 3123 – 3127 Vol.5.

[8] N. Guo, B. Sadler, and R. Qiu, "Reduced-complexity uwb time-reversal techniques and experimental results," *Wireless Communications, IEEE Transactions on*, vol. 6, no. 12, pp. 4221 –4226, Dec. 2007.

[9] K. Witrisal, E. Leitinger, P. Meissner, and D. Arnitz, "Cognitive radar for the localization of RFID transponders in dense multipath environments," in *Radar (RadarCon), 2013 IEEE International Conference on*, April 2013.

[10] P. Meissner, D. Arnitz, T. Gigl, and K. Witrisal, "Analysis of an indoor UWB channel for multipath-aided localization," in *Ultra-Wideband (ICUWB), 2011 IEEE International Conference on*, Sept. 2011, pp. 565 –569.

[11] A. Molisch, "Ultra-wide-band propagation channels," *Proceedings of the IEEE*, vol. 97, no. 2, pp. 353 –371, Feb. 2009.

[12] H. L. Van Trees, *Detection, Estimation and Modulation, Part I*. Wiley Press, 1968.

[13] J. Karedal, S. Wyne, P. Almers, F. Tufvesson, and A. Molisch, "A measurement-based statistical model for industrial ultra-wideband channels," *Wireless Communications, IEEE Transactions on*, vol. 6, no. 8, pp. 3028–3037, Aug.